




Laguerre-Gaussian transform for rotating image processing

DAN WEI,^{1,4} JIANTAO MA,^{1,4} TIANXIN WANG,¹ CHUAN XU,¹
SHINING ZHU,^{1,2} MIN XIAO,^{1,2,3} AND YONG ZHANG^{1,2,*} 

¹National Laboratory of Solid State Microstructures, College of Engineering and Applied Sciences, and School of Physics, Nanjing University, Nanjing 210093, China

²Collaborative Innovation Center of Advanced Microstructures, Nanjing University, Nanjing 210093, China

³Department of Physics, University of Arkansas, Fayetteville, Arkansas 72701, USA

⁴These authors contribute equally to this work

*zhangyong@nju.edu.cn

Abstract: In practical applications, it is often crucial to track high-speed rotating objects. However, the traditional Fourier transform techniques are not applicable under such circumstances because the Fourier spectrum of a rotating object is changing. Here, we propose a Laguerre-Gaussian (LG) transform to analyze the rotating object. The rotation provides a feasible way to acquire a LG-mode spectrum, which does not change even the object working at a high rotating speed. By analyzing the LG spectrum, one can perform image processing such as reconstruction, edge enhancement, and pattern replication. The LG transform makes it convenient for real-time monitoring of industrial and astronomical objects.

© 2020 Optical Society of America under the terms of the [OSA Open Access Publishing Agreement](#)

1. Introduction

FT decomposes a temporal signal into its constituent frequencies. Because many linear operations including differentiation and convolution are much easier to perform in the frequency domain, FT has been widely applied in analysis of differential equations, FT spectroscopy, and signal processing [1]. In Fourier optics, FT from an optical pattern to its spatial frequency components can be readily achieved by using an optical lens [2]. Based on such optical FT, powerful tools, such as image reconstruction, edge recognition, spatial filtering, computer generated hologram, and image compression [2–4], have been developed for image processing schemes. However, in real-time monitoring of a rotating object (such as a biological molecule, industrial centrifuge and turbine, and an astronomical object), the typical optical FT techniques would not work as efficiently as usual. Since its Fourier spatial frequency spectrum is changing along with the rotating object, FT-based image processing schemes become complicated and time consuming. In this article, we propose and experimentally demonstrate to use a Laguerre-Gaussian (LG) transform of a rotating object to overcome this problem. The obtained LG spectrum does not vary with the rotation, which provides great convenience and a nature way for further image processing of a fast-rotating object.

Figure 1 compares the FT and LG transforms of a spatial image. The fundamental difference is the basis used to decompose the target spatial pattern. In FT, the optical image of an object is considered as a superposition of plane waves and the aim is to convert the image into the spatial frequency spectrum. In LG transform, the basis to decompose an optical image is chosen to be the LG modes. LG modes are the Eigen solutions of the paraxial Helmholtz equation [5], which are characterized by an azimuthal index l and a radial index p . Therefore, LG modes are capable to represent the spatial structure of a transverse field under paraxial approximation [6,7]. LG

modes can be expressed as

$$\begin{aligned}
 & LG_{p,l}(r, \phi) \\
 &= \sqrt{\frac{2p!}{\pi(p+|l|)!}} \frac{1}{\omega_0} \left(\sqrt{2} \frac{r}{\omega_0} \right)^{|l|} L_p^{|l|} \left(2 \frac{r^2}{\omega_0^2} \right) \\
 &\exp\left(-\frac{r^2}{\omega_0^2}\right) \exp(il\phi) \\
 &= LG_{p,l}(r) \exp(il\phi).
 \end{aligned} \tag{1}$$

Here, $L_p^{|l|}$ are the Laguerre polynomials, r is the radial cylindrical coordinate, ϕ is the azimuthal angle, and ω_0 is the beam waist. $LG_{p,l}(r)$ is the radial term of an LG mode. Various methods have been proposed to generate LG modes, such as spiral phase plates [8], spatial light modulators, Q-plates [9], and cavities [10–12]. Because the LG basis naturally features circular symmetry, rotating the object does not change the measured LG spectrum in such case, even when the object rotates at a high speed. Such unique advantage makes the basis of LG modes an ideal candidate to analyze a rotating object.

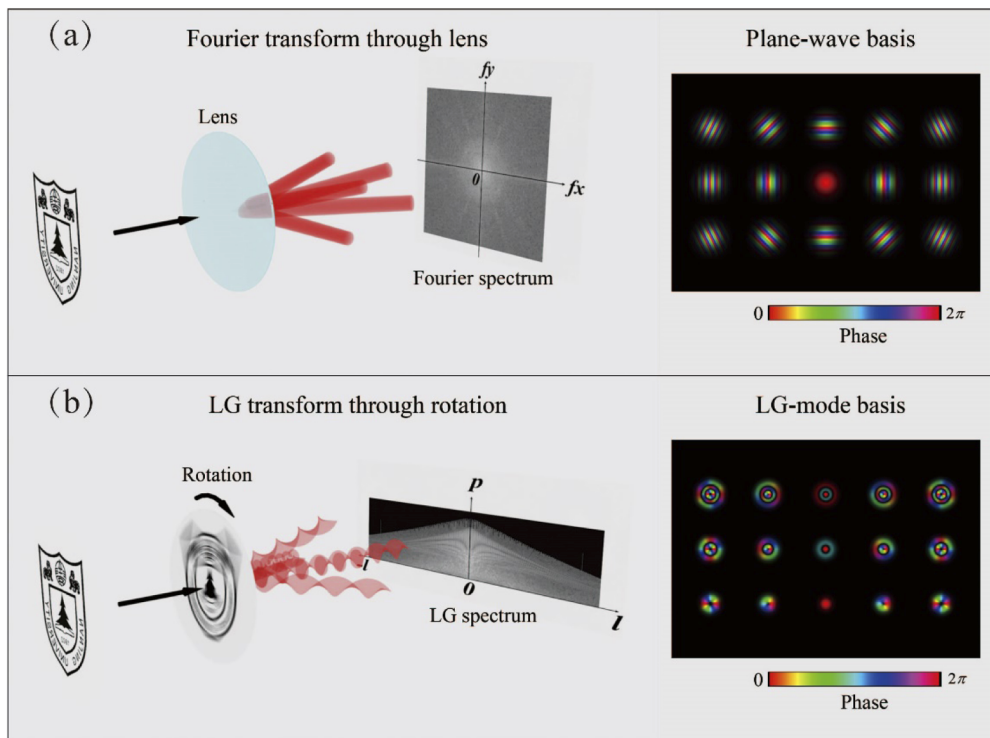


Fig. 1. Comparison of FT and LG transforms. (a) In FT transform, a spatial image is decomposed into its spatial frequency spectrum by use of an optical lens. However, if the image is rotating, the FT spectrum is changing. (b) In LG transform, an image is considered as a superposition of various LG modes. Rotating the image is an effective operation to obtain its LG spectrum, which does not change even the object has a fast rotary speed.

In addition, rotation is a feasible operation to obtain LG spectrum, which is similar to the function of a lens in optical FT. The azimuthal index l of an LG mode is associated with the orbital angular momentum of light [13], which has been widely investigated in optical communications [14,15], gravitational-wave detection [16], and nonlinear and quantum optics [17,18]. Based

on the rotational Doppler effect, i.e., the Doppler frequency shift from a spinning object being proportional to l [19–28], one can have the distribution of l index [25,27]. The l spectrum reflects the azimuthal structure of the object, which can be used to measure the rotary speed [21,22], azimuthal angle [29] and azimuthal symmetry [5,6,25,28,30]. However, this is not enough to reconstruct a full image because of the loss of radial information. To fix this problem, we develop an effective method to obtain both azimuthal index l and radial index p for constructing the complete LG spectrum.

2. Theoretical analysis of Laguerre-Gaussian transform

Assume that the target rotating field at $t = 0$ is described as $E(r, \phi)$. By using the LG-mode basis, $E(r, \phi)$ can be written as

$$\begin{aligned} E(r, \phi) &= \sum_l \sum_p A_{p,l} LG_{p,l}(r) \exp(il\phi) \\ &= \sum_l b_l(r) \exp(il\phi), \end{aligned} \quad (2)$$

where $A_{p,l}$ is the complex LG spectrum of $E(r, \phi)$ with $\sum_l \sum_p |A_{p,l}|^2 = 1$. Here, we define

$$b_l(r) = \sum_p A_{p,l} LG_{p,l}(r), \quad (3)$$

which represents the overall contributions from the LG modes with the same l but different p . $b_l(r)$ generally varies with radius r in a complex image.

When the object rotates at an angular frequency Ω , each LG component has a frequency shift $l\Omega$ according to the rotational Doppler effect [19–28]. Then, the rotating field can be written as

$$E(r, \phi, t) = \sum_l b_l(r) \exp(il\phi) \exp(il\Omega t), \quad (4)$$

where t denotes time. One can measure $E(r, \phi_0, t)$ by setting a 1D detector array or scanning a single-point detector (SPD) along a certain azimuthal angle ϕ_0 . $I_n(t)$ is the intensity detected at radius r_n ($n \in [1, 2, 3 \dots N]$), where N is the number of radial sampling point. Considering that the size of a single detector is much smaller than the size of image, the measured field $E(r_n, \phi_0, t)$ can be expressed as

$$E(r_n, \phi_0, t) \approx \sqrt{\frac{I_n(t)}{s}} = \sum_l b_l(r_n) \exp(il\phi_0) \exp(il\Omega t), \quad (5)$$

where s is the area of a single detector. Through time Fourier transform, $b_l(r_n)$ (with l being 0, $\pm 1, \pm 2, \dots$) is calculated from

$$b_l(r_n) = \frac{\exp(-il\phi_0)}{T} \int_0^T E(r_n, \phi_0, t) \exp(-il\Omega t) dt, \quad (6)$$

where $T = \frac{2\pi}{\Omega}$ is the rotation period. From Eq. (3), $b_l(r_n)$ with a given l can form the following multivariate linear equations,

$$\begin{cases} b_l(r_1) = A_{l,0} LG_{l,0}(r_1) + A_{l,1} LG_{l,1}(r_1) + \dots + A_{l,p} LG_{l,p}(r_1) \\ b_l(r_2) = A_{l,0} LG_{l,0}(r_2) + A_{l,1} LG_{l,1}(r_2) + \dots + A_{l,p} LG_{l,p}(r_2) \\ \vdots \\ b_l(r_N) = A_{l,0} LG_{l,0}(r_N) + A_{l,1} LG_{l,1}(r_N) + \dots + A_{l,p} LG_{l,p}(r_N). \end{cases} \quad (7)$$

When $N > p + 1$, Eq. (7) forms an undetermined system and $A_{l,0}, A_{l,1}, \dots, A_{l,p}$ can be calculated by least square fitting. Then, one can obtain the complete LG spectrum by solving Eq. (7) with different l . Note that the fitting parameters such as beam waist and truncation mode number of LG mode are optimized [31].

3. Experimental results

In the experiment, the rotating pattern is generated by a computer-controlled digital micromirror device (DMD) [Fig. 2(a)]. The rotating period is set to be 50 ms. After using a 4f imaging system

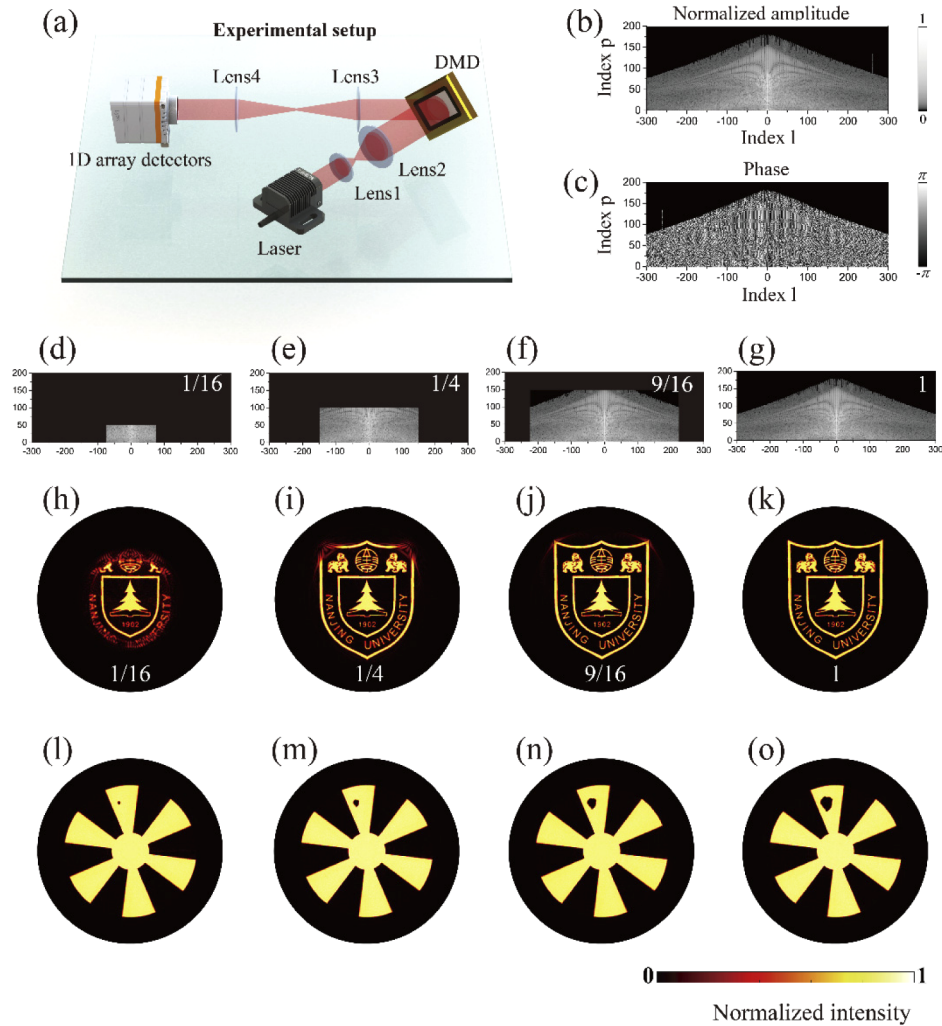


Fig. 2. The experimental results. (a) shows the experimental setup. A series of amplitude patterns are playing on the DMD to mimic a rotating object. The rotating field is detected by a 1D array detector, which is set at an azimuthal angle ϕ_0 . (b) and (c) are the amplitude and phase of the measured LG spectrum from a rotating emblem of Nanjing University. (d)-(g) show used portions of the LG spectrum to reconstruct the emblems displayed in (h)-(k), respectively. (l)-(o) exhibit an example of monitoring the defect evolution in a working fan. The reconstructed frames clearly show a growing hole. See movies in [Visualization 1](#) and [Visualization 2](#).

to amplify the pattern, a rotating image (~ 1000 dpi) is detected by a 1D detector array. Figure 2 depicts the reconstruction of a rotating emblem of Nanjing University. See movie in [Visualization 1](#). Figures 2(b) and 2(c) show the amplitude and phase of the measured LG spectrum. The used LG basis includes about 10^5 LG components with l ranging from -300 to 300 and p from 0 to 180. Figures 2(h)–2(k) show the reconstructed images using 1/16, 1/4, 9/16 and the entirely measured LG spectrum, respectively. As shown in Fig. 2(i), the image can be reproduced well using 1/4 of the measured LG spectrum because most of the image information are provided by the relatively lower-order LG components. If enlarging the scale of the selected LG modes [Figs. 2(f) and 2(g)], the image quality can be further increased [Figs. 2(j) and 2(k)].

Considering that the information captured within one rotation period is enough to reconstruct a full image, this technique can be used for certain practical task, i.e., real-time monitoring the dynamic evolution of a rotating pattern. The minimal acquisition time is equal to the rotational period. For example, we track a hole defect in a working fan. Figures 2(l)–2(o) present four continuous frames of the fan reconstructed from the real-time LG spectra. One can clearly see the growing process of the hole defect when the fan is still at work (see movie in [Visualization 2](#)). Interestingly, faster the fan rotates, more frames per second can be achieved in principle. Such unique function of LG transform is very helpful for the in-situ monitoring of the status of a rotating object when it is inconvenient or too expensive to completely stop running it for inspection.

4. Rotating image processing

Figure 3 shows several typical image processing schemes by selectively modulating the LG spectrum. Figures 3(a)–3(e) demonstrate the edge enhancement of a fan by performing differential operations on the LG spectrum. The azimuthal and radial edge enhancements [Fig. 3(c) and 3(d)] are achieved by choosing ϕ and r as differential variables, respectively, i.e.,

$$\begin{aligned} & \sum_l \sum_p A_{p,l} \left(\frac{\partial LG_{p,l}(r,\phi)}{r \partial \phi} \right) \\ & = \sum_l \sum_p i_r^l A_{p,l} LG_{p,l}(r,\phi) = E_\phi, \end{aligned} \quad (8)$$

$$\begin{aligned} & \sum_l \sum_p A_{p,l} \left(\frac{\partial LG_{p,l}(r,\phi)}{\partial r} \right) = \\ & \sum_l \sum_p \left[\frac{|l|}{r} - \frac{2r}{\omega_0^2} - \frac{4r}{\omega_0^2} \frac{L_p^{|l|+1} \left(\frac{2r^2}{\omega_0^2} \right)}{L_p^{|l|} \left(\frac{2r^2}{\omega_0^2} \right)} \right] A_{p,l} LG_{p,l}(r,\phi) = E_r, \end{aligned} \quad (9)$$

By combining Eqs. (8) and (9), we obtain the complete edge enhancement [Fig. 3(e)], i.e.,

$$\begin{aligned} & \sum_l \sum_p A_{p,l} \left(\frac{\partial LG_{p,l}(r,\phi)}{\partial r} + \frac{\partial LG_{p,l}(r,\phi)}{r \partial \phi} \right) \\ & = \sum_l \sum_p \left[\frac{|l|}{r} - \frac{2r}{\omega_0^2} - \frac{4r}{\omega_0^2} \frac{L_p^{|l|+1} \left(\frac{2r^2}{\omega_0^2} \right)}{L_p^{|l|} \left(\frac{2r^2}{\omega_0^2} \right)} + i_r^l \right] A_{p,l} LG_{p,l}(r,\phi) \\ & = E_r + E_\phi = E_{r,\phi}. \end{aligned} \quad (10)$$

Here, E_ϕ , E_r , and $E_{r,\phi}$ represent the obtained field after azimuthal, radial and entire edge enhancements, respectively.

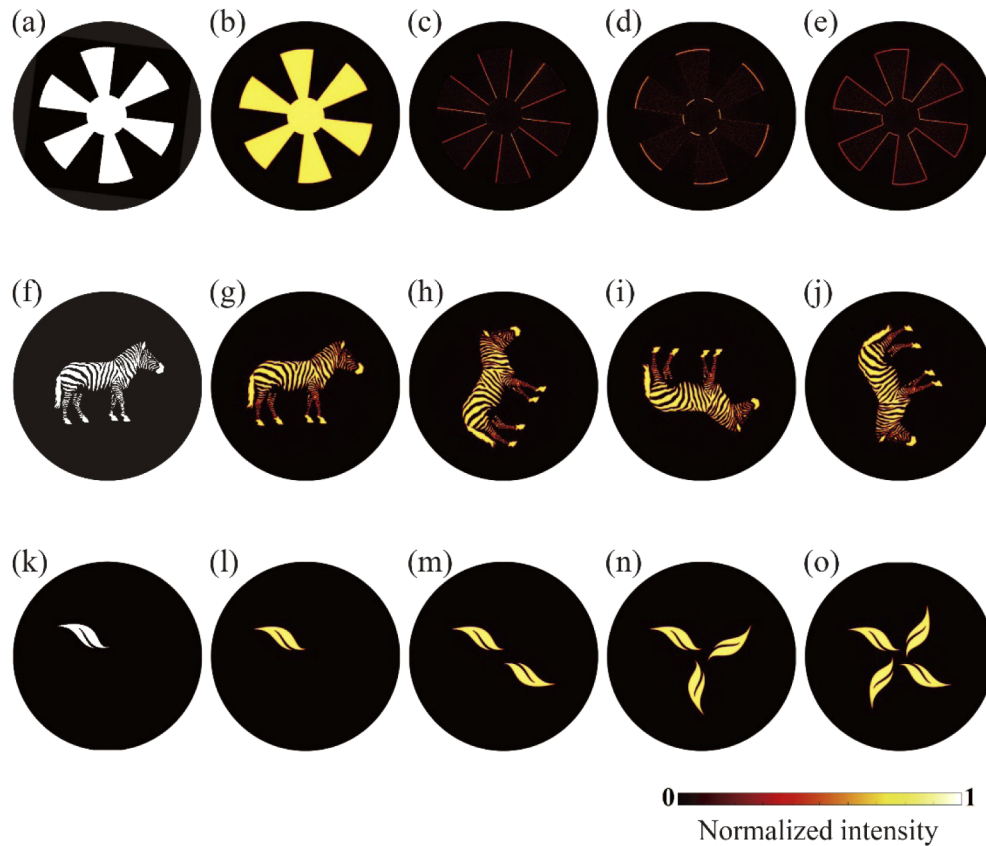


Fig. 3. Image processing by manipulating the LG spectrum. When the original objects, i.e., a fan (a), a zebra (f), and a leaf (k), are rotating, we can well reconstruct their images in (b), (g), and (l) by using the LG transform method. Azimuthal and radial edge enhancements in c-e can be achieved by choosing either ϕ (c), r (d), or both (e) as differential variables. Note that edge enhancement can be applied to arbitrary images. Symmetric operations can be performed by adding a phase $l\Delta\phi$ into the LG spectrum (h), conjugating the phase of the LG spectrum (i), or combining them together (j). Pattern replication can be realized by selecting the LG components with their l indices being the multiple of 2 (m), 3 (j), or 4 (o).

Figures 3(f)–3(j) present the symmetric operations of a zebra image. The rotation operation is achieved by simply adding a phase $l\Delta\phi$ to each LG mode, i.e.,

$$\begin{aligned}
 & \sum_l \sum_p A_{p,l} LG_{p,l}(r, \phi) \exp(il\Delta\phi) \\
 &= \sum_l \sum_p A_{p,l} LG_{p,l}(r) \exp(il\phi) \exp(il\Delta\phi) \\
 &= \sum_l \sum_p A_{p,l} LG_{p,l}(r) \exp[il(\phi + \Delta\phi)] \\
 &= E(r, \phi + \Delta\phi).
 \end{aligned} \tag{11}$$

We use $\Delta\phi = 60^\circ$ for example in Fig. 3(h). The reflection operation [Fig. 3(i)] is realized by conjugating the spiral phase of each LG component, which is described as

$$\begin{aligned}
 & \sum_l \sum_p A_{p,l} [LG_{p,l}(r, \phi)]^* \\
 &= \sum_l \sum_p A_{p,l} LG_{p,l}(r) \exp(-il\phi) \\
 &= E(r, -\phi).
 \end{aligned} \tag{12}$$

By combining Eqs. (11) and (12) together, the image can be folded along an arbitrary axis. This operation can be described as

$$\begin{aligned}
 & \sum_l \sum_p A_{p,l} [LG_{p,l}(r, \phi)]^* \exp(il\Delta\phi) \\
 &= \sum_l \sum_p A_{p,l} LG_{p,l}(r) \exp[il(-\phi + \Delta\phi)] \\
 &= E(r, -\phi + \Delta\phi).
 \end{aligned} \tag{13}$$

The image is folded along $-\Delta\phi/2$. Figure 3(j) shows an example with $\Delta\phi = 60^\circ$.

Figures 3(k)–3(o) depict how to replicate a pattern by manipulating the LG spectrum. The pattern replication is realized by superposing the LG modes with their l indices being the multiple of an integer m , i.e.,

$$\sum_{l=km} \sum_p A_{p,l} LG_{p,l}(r, \phi) = E^m, \tag{14}$$

where $k = \pm 1, \pm 2, \pm 3 \dots$ and E^m is the obtained field after pattern replication operation. The original image is a single leaf [Fig. 3(k)]. Through picking out the LG modes with their l indices being the multiple of 2, 3, or 4, one can obtain double [Fig. 3(m)], triple [Fig. 3(n)] or quadruple leaves [Fig. 3(o)] respectively.

5. Experiment with SPD

In addition, our method can be performed by using one SPD, which, in comparison to array detectors, has the advantages of faster response time and broader frequency bandwidth, and therefore, is capable to track higher-speed rotating object. The schematic experimental setup is shown in Fig. 4(a). A chopper covered by the numbers from 1 to 5 serves as the rotating object. It works at 100 Hz frequency. The rotating optical field is detected by a 1-MHz SPD, which scans along the radial direction. The reconstructed image using the LG spectrum is shown in Fig. 4(b), which well reproduces the original five numbers. In theory, the maximal measurable rotation speed of our system is up to 2,000 revolutions per second, which can be further enhanced by increasing the bandwidth of the used SPD.

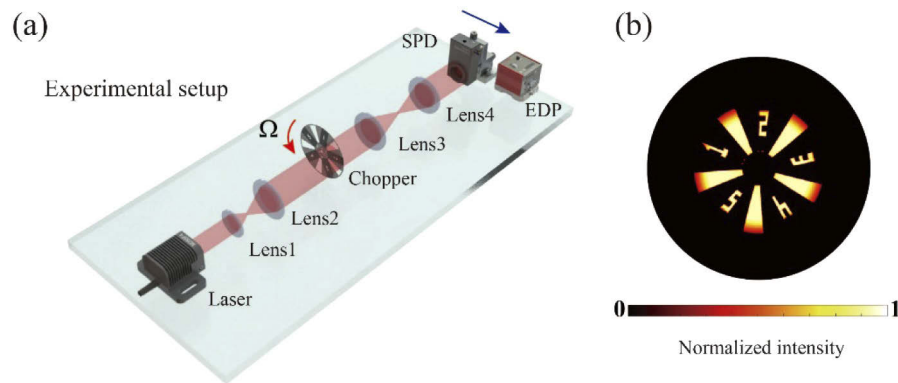


Fig. 4. Experimental configuration with SPD. (a), The experimental setup. The object is a chopper covered by numbers 1-5, which rotates at 100 Hz frequency. The SPD is scanned along the radial direction. (b), The reconstructed image. SPD: single-point detector. EDP: electric displacement platform.

6. Conclusion

We have proposed and experimentally demonstrated the use of LG transform for detecting a rotating object. Our method can have profound applications in scientific research and industry. For example, it provides an effective and powerful platform for in-situ monitoring of aero-engine, super-centrifuge, and gas turbine, which typically work under extreme conditions such as high pressure, high temperature, and high vacuum. Several unique advantages distinguish our method from traditional FT techniques in detecting a rotating object. First, the LG spectrum of a rotating object does not change, which provides a great convenience for real-time image reconstruction and analysis. Second, rotation itself is a feasible way to measure the LG spectrum. So, the experimental measurement system is simple and effective. Third, a commercial SPD can satisfy the detection requirement. In comparison to image cameras, the performance of low-cost SPDs are generally superior in detection efficiency, bandwidth, and response time. In addition, the demonstrated SPD configuration can be further extended to cover infrared, THz, and X-ray bands, where it is expensive or impossible to acquire a high-quality camera. Therefore, the proposed LG transform can truly provide a practical platform to detect and monitor high-speed rotating objects in biology, industry and astronomy.

Funding

National Key Research and Development Program of China (2017YFA0303703, 2016YFA0302500); National Natural Science Foundation of China (91950206, 11874213); Nanjing University Innovation and Creative Program for PhD candidate (CXCY17-27); Natural Science Foundation of Jiangsu Province (BK20180322); Fundamental Research Funds for the Central Universities (1480605201, 14380105).

Acknowledgment

We thank Jianping Ding for useful discussion.

Disclosures

The authors declare no conflicts of interest.

References

1. A. V. Oppenheim, A. S. Willsky, and W. S. Hamid, *Signals and Systems*: 2nd Edition (Pearson Education, 1996).
2. J. W. Goodman, *Introduction To Fourier Optics*, 3rd Edition (Roberts Company, 1968).
3. Z. Zhang, X. Ma, and J. Zhong, "Single-pixel imaging by means of Fourier spectrum acquisition," *Nat. Commun.* **6**(1), 6225 (2015).
4. X. Qiu, F. Li, W. Zhang, Z. Zhu, and L. Chen, "Spiral phase contrast imaging in nonlinear optics: seeing phase objects using invisible illumination," *Optica* **5**(2), 208 (2018).
5. G. Molina-Terriza, J. P. Torres, and L. Torner, "Management of the angular momentum of light: preparation of photons in multidimensional vector states of angular momentum," *Phys. Rev. Lett.* **88**(1), 013601 (2001).
6. D. S. Simon and A. V. Sergienko, "Two-photon spiral imaging with correlated orbital angular momentum states," *Phys. Rev. A* **85**(4), 043825 (2012).
7. L. Torner, J. P. Torres, and S. Carrasco, "Digital spiral imaging," *Opt. Express* **13**(3), 873–881 (2005).
8. M. W. Beijersbergen, R. P. C. Coerwinkel, M. Kristensen, and J. P. Woerdman, "Helical-wavefront laser beams produced with a spiral phaseplate," *Opt. Commun.* **112**(5-6), 321–327 (1994).
9. L. Marrucci, C. Manzo, and D. Paparo, "Optical spin-to-orbital angular momentum conversion in inhomogeneous anisotropic media," *Phys. Rev. Lett.* **96**(16), 163905 (2006).
10. D. Wei, Y. Cheng, R. Ni, Y. Zhang, X. Hu, S. Zhu, and M. Xiao, "Generating Controllable Laguerre-Gaussian Laser Modes Through Intracavity Spin-Orbital Angular Momentum Conversion of Light," *Phys. Rev. Appl.* **11**(1), 014038 (2019).
11. X. Cai, J. Wang, M. J. Strain, B. Johnson-Morris, J. Zhu, M. Sorel, J. L. O'Brien, M. G. Thompson, and S. Yu, "Integrated Compact Optical Vortex Beam Emitters," *Science* **338**(6105), 363–366 (2012).
12. L. Feng, M. Ayache, J. Huang, Y.-L. Xu, M.-H. Lu, Y.-F. Chen, Y. Fainman, and A. Scherer, "Nonreciprocal Light Propagation in a Silicon Photonic Circuit," *Science* **333**(6043), 729–733 (2011).
13. L. Allen, M. W. Beijersbergen, R. J. C. Spreeuw, and J. P. Woerdman, "Orbital angular momentum of light and the transformation of Laguerre-Gaussian laser modes," *Phys. Rev. A* **45**(11), 8185–8189 (1992).
14. N. Bozinovic, Y. Yue, Y. Ren, M. Tur, P. Kristensen, H. Huang, A. E. Willner, and S. Ramachandran, "Terabit-Scale Orbital Angular Momentum Mode Division Multiplexing in Fibers," *Science* **340**(6140), 1545–1548 (2013).
15. J. Wang, J.-Y. Yang, I. M. Fazal, N. Ahmed, Y. Yan, H. Huang, Y. Ren, Y. Yue, S. Dolinar, M. Tur, and A. E. Willner, "Terabit free-space data transmission employing orbital angular momentum multiplexing," *Nat. Photonics* **6**(7), 488–496 (2012).
16. L. Carbone, C. Bogan, P. Fulda, A. Freise, and B. Willke, "Generation of High-Purity Higher-Order Laguerre-Gauss Beams at High Laser Power," *Phys. Rev. Lett.* **110**(25), 251101 (2013).
17. A. Mair, A. Vaziri, G. Weihs, and A. Zeilinger, "Entanglement of the orbital angular momentum states of photons," *Nature* **412**(6844), 313–316 (2001).
18. D. Wei, C. Wang, X. Xu, H. Wang, Y. Hu, P. Chen, J. Li, Y. Zhu, C. Xin, X. Hu, Y. Zhang, D. Wu, J. Chu, S. Zhu, and M. Xiao, "Efficient nonlinear beam shaping in three-dimensional lithium niobate nonlinear photonic crystals," *Nat. Commun.* **10**(1), 4193 (2019).
19. J. Courtial, K. Dholakia, D. A. Robertson, L. Allen, and M. J. Padgett, "Measurement of the Rotational Frequency Shift Imparted to a Rotating Light Beam Possessing Orbital Angular Momentum," *Phys. Rev. Lett.* **80**(15), 3217–3219 (1998).
20. J. Courtial, D. A. Robertson, K. Dholakia, L. Allen, and M. J. Padgett, "Rotational Frequency Shift of a Light Beam," *Phys. Rev. Lett.* **81**(22), 4828–4830 (1998).
21. M. P. Lavery, F. C. Speirits, S. M. Barnett, and M. J. Padgett, "Detection of a spinning object using light's orbital angular momentum," *Science* **341**(6145), 537–540 (2013).
22. Y. W. Zhai, S. Y. Fu, C. Yin, H. Zhou, and C. Q. Gao, "Detection of angular acceleration based on optical rotational Doppler effect," *Opt. Express* **27**(11), 15518–15527 (2019).
23. F. Li, T. Xu, W. Zhang, X. Qiu, X. Lu, and L. Chen, "Optical images rotation and reflection with engineered orbital angular momentum spectrum," *Appl. Phys. Lett.* **113**(16), 161109 (2018).
24. S. Xiao, L. Zhang, D. Wei, F. Liu, Y. Zhang, and M. Xiao, "Orbital angular momentum-enhanced measurement of rotation vibration using a Sagnac interferometer," *Opt. Express* **26**(2), 1997–2005 (2018).
25. W. Zhang, J. Gao, D. Zhang, Y. He, T. Xu, R. Fickler, and L. Chen, "Free-Space remote sensing of rotation at the photon-counting level," *Phys. Rev. Appl.* **10**(4), 044014 (2018).
26. H. Zhou, D. Fu, J. Dong, P. Zhang, and X. Zhang, "Theoretical analysis and experimental verification on optical rotational Doppler effect," *Opt. Express* **24**(9), 10050–10056 (2016).
27. H. L. Zhou, D. Z. Fu, J. J. Dong, P. Zhang, D. X. Chen, X. L. Cai, F. L. Li, and X. L. Zhang, "Orbital angular momentum complex spectrum analyzer for vortex light based on the rotational Doppler effect," *Light: Sci. Appl.* **6**(4), e16251 (2017).
28. Y. W. Zhai, S. Y. Fu, J. Q. Zhang, Y. L. Lv, H. Zhou, and C. Q. Gao, "Remote detection of a rotator based on rotational Doppler effect," *Appl. Phys. Express* **13**(2), 022012 (2020).
29. G. Xie, H. Song, Z. Zhao, G. Milione, Y. Ren, C. Liu, R. Zhang, C. Bao, L. Li, Z. Wang, K. Pang, D. Starodubov, B. Lynn, M. Tur, and A. E. Willner, "Using a complex optical orbital-angular-momentum spectrum to measure object parameters," *Opt. Lett.* **42**(21), 4482–4485 (2017).
30. B. Jack, M. J. Padgett, and S. Franke-Arnold, "Angular diffraction," *New J. Phys.* **10**(10), 103013 (2008).

31. J. Ma, D. Wei, H. Yang, Y. Zhang, and M. Xiao, "Optical image decomposition and noise processing based on Laguerre-Gaussian modes," arXiv:2005.07701 (2020).